In situ catalytic reforming of plastic pyrolysis vapors using MSW incineration ashes

Ahamed, Ashiq; Liang, Lili; Chan, Wei Ping; Tan, Preston Choon Kiat; Yip, Nicklaus Tze Xuan; Bobacka, Johan; Veksha, Andrei; Yin, Ke; Lisak, Grzegorz

Published in:
Environmental Pollution

DOI:
10.1016/j.envpol.2021.116681

Published: 01/05/2021

Document Version
Accepted author manuscript

Document License
CC BY-NC-ND

In situ catalytic reforming of plastic pyrolysis vapors using MSW incineration ashes

*Ashiq Ahamed[a,b], Lili Liang[c,d], Wei Ping Chan[a], Preston Choon Kiat Tan[a,c], Nicklaus Tze Xuan Yip[c], Johan Bobacka[b], Andrei Veksha[a], Ke Yin[a,e], Grzegorz Lisak[a,c,]**

[a] *Residues and Resource Reclamation Centre, Nanyang Environment and Water Research Institute, Nanyang Technological University, 1 Cleantech Loop, CleanTech One, Singapore 637141 Singapore.*

[b] *Laboratory of Molecular Science and Engineering, Johan Gadolin Process Chemistry Centre, Åbo Akademi University, FI-20500 Turku, Finland.*

[c] *School of Civil and Environmental Engineering, Nanyang Technological University, Singapore 639798, Singapore.*

[d] *Interdisciplinary Graduate Program, Nanyang Technological University, 1 Cleantech Loop, CleanTech One, Singapore 637141 Singapore.*

e Department of Environmental Engineering, College of Biology and the Environment, Nanjing Forestry University, 159 Longpan Road, Nanjing 210037, China

**Corresponding author: g.lisak@ntu.edu.sg (G.Lisak)*

Abstract

The valorization of municipal solid waste incineration bottom and fly ashes (IBA and IFA) as catalysts for thermochemical plastic treatment was investigated. As-received, calcined, and Ni-loaded ashes prepared via hydrothermal synthesis were used as low-cost waste-derived catalysts for in-line upgrading of volatile products from plastic pyrolysis. It was found that both IBA and air pollution control IFA (APC) promote selective production of BTEX compounds (i.e., benzene, toluene, ethylbenzene, and xylenes) without significantly affecting the formation of other gaseous

and liquid species. There was insignificant change in the product distribution when electrostatic precipitator IFA (ESP) was used, probably due to the lack of active catalytic species. Calcined APC (C-APC) demonstrated further improvement in the BTEX yield that suggested the potential to enhance the catalytic properties of ashes through pre-treatment. By comparing with the leaching limit values stated in the European Council Decision 2003/33/EC for the acceptance of hazardous waste at landfills, all the ashes applied remained in the same category after the calcination and pyrolysis processes, except the leaching of Cl^- from the ESP, which was around the borderline. Therefore, the use of ashes in catalytic reforming application do not significantly deteriorate their metal leaching behavior. Considering its high catalytic activity towards BTEX formation, C-APC was loaded with Ni at 15 and 30 wt%. The Ni-loading favored an increase in overall oil yield, while reducing the gas yield when compared to the benchmark Ni loaded ZSM catalyst. However, Ni addition also caused the formation of more heavier hydrocarbons (C20-C35) that would require post-treatment to recover favorable products like BTEX.

Capsule: Application of MSW incineration ashes in catalytic reforming of plastic pyrolysis vapor promoted selective BTEX yield without altering the leaching behavior of the ashes.

Keywords: Pyrolysis, catalytic reforming, plastic, IBA, IFA.

Nomenclature:

APC	Air pollution control fly ash
BET	Brunauer–Emmett–Teller
BTEX	Benzene, Toluene, Ethylbenzene, p- and o- xylene
C-APC	Calcined air pollution control fly ash
C-ESP	Calcined electrostatic precipitator fly ash

C-IBA	Calcined incineration bottom ash
DI	Deionized
ESP	Electrostatic precipitator fly ash
FESEM-EDS	Field emission scanning electron microscopy with energy dispersed spectroscopy
GC-MS	Gas chromatography - mass spectrometry
HDPE	High density polyethylene
HZSM-5	Protonated type of Zeolite Socony Mobil-5
IBA	Incineration bottom ash
ICP-MS	Inductively coupled plasma - mass spectrometry
ICP-OES	Inductively coupled plasma - optical emission spectrometry
IFA	Incineration fly ash
LDPE	Low density polyethylene
LOI	Loss on ignition
MSW	Municipal solid waste
PE	Polyethylene
PP	Polypropylene
PTFE	Polytetrafluoroethylene
R-APC	Raw air pollution control fly ash
R-ESP	Raw electrostatic precipitator fly ash
R-IBA	Raw incineration bottom ash
XRD	X-ray diffraction
ZSM-5	Zeolite Socony Mobil-5

15Ni-APC	15 wt% Nickel loaded C-APC
15Ni-ZSM	15 wt% Nickel loaded ZSM-5
30Ni-APC	30 wt% Nickel loaded C-APC

1. Introduction

Plastic pyrolysis is a promising technology for the treatment of mixed plastic waste. During pyrolysis, plastic feedstock is thermally decomposed in the absence of oxygen into volatile organic vapors, which are then condensed to produce pyrolysis oil and non-condensable gas products. Catalytic reforming is an add-on process to plastic pyrolysis, where the pyrolysis vapors are exposed to a bed of catalyst, thereby, reforming the product formation. Catalytic reforming of pyrolysis vapors exhibits various advantages including, increased selectivity, superior product yield, avoidance of undesirable products formation, and production of liquid products with a lower boiling point (Saraçoğlu et al., 2017; Iliopoulou et al., 2012; Zheng et al., 2017). The catalysts predominantly used in reforming application are of natural origin including zeolites, clay, and silica-alumina (Auxilio et al., 2017; Wang & Wang, 2011; Miandad et al., 2016). Further, the catalysts require periodical replacement due to the irreversible deactivation attributed to poisoning, leaching, and sintering (Alekseeva (Bykova) et al., 2019), adding to the costs of the process and its environmental burden.

The municipal solid waste (MSW) incineration process results in residual ashes commonly known as incineration bottom and fly ashes (IBA and IFA, respectively). Incineration ashes are typically landfilled as hazardous or non-hazardous wastes, depending on their pollutants leaching behavior. In order to minimize the waste disposal, there is an ongoing research and development to valorize ash usage in various applications including chemical looping combustion (Yin et al., 2021; Cudjoe

and Acquah, 2021), carbon capture (Viet et al., 2020), industrial wastewater treatment (Lei et al., 2020), construction and land reclamation (Dou et al., 2017; Chan et al., 2018; Yin et al., 2018). One of the promising areas of ash utilization is the development of catalysts. IBA generated from the incineration of MSW was explored as a catalyst support in syngas production from biomass (Ashok et al., 2018). The study demonstrated superior catalytic performance of Ni loaded IBA for the conversion of toluene to gas products that was attributed to the presence of high amounts of reducible surface Ni species and basicity of the support. Huang et al. (2016) reported superior catalytic reforming activity of calcined MSW IBA for converting toluene to H_2 when compared to thermal cracking. This was attributed to the presence of CaO, MgO, and Fe_2O_3 compounds. In other studies, significant increase in gas product was reported for the catalytic reforming of biomass pyrolysis vapor using coal, refuse derived fuel, and waste tire combustion ashes attributed to the inherent metal content, and Ni impregnation on these ashes resulted in further improvement (~20%) of H_2 yield (Al-Rahbi and Williams, 2019). Wang et al. (2014) investigated the catalytic steam reforming of acetic acid and phenol using a 15 wt% Ni-loaded coal ash catalyst. Ni addition improved the conversion rate from 57% and 26% to 98% and 83% for acetic acid and phenol, respectively. These examples show that the incineration ashes have high potential to be applied in catalytic upgrading of biomass-derived gases, maximizing the resource recovery from these wastes (Al-Rahbi and Williams, 2019). In plastic pyrolysis application, coal fly ash derived amorphous silica alumina catalysts fused with NaOH demonstrated comparable catalytic potential to commercial catalysts by producing low boiling point oil products from low density polyethylene (LDPE) pyrolysis (Na et al., 2006). Calcined coal power plant fly ash (800 °C, 5 h) produced almost twice the benzene, toluene, ethylbenzene, and xylene contents in the waste polyethylene (PE) pyrolysis when compared to thermal pyrolysis due to the high surface area and silica alumina

ratio leading to higher selectivity (Gaurh and Pramanik, 2018). While the studies discussed above demonstrated the application of ashes from MSW as catalysts for reforming of biomass-derived volatile compounds, their feasibility for pyrolysis oil upgrading from plastics has not been investigated.

Plastic pyrolysis results in the formation of a complex mixture of hydrocarbons represented by paraffins, olefins, naphthenes and aromatics. In order to obtain a superior pyrolysis oil quality, catalytic pyrolysis and reforming studies focused on the improvement of the yield of BTEX compounds (i.e. benzene, toluene, ethylbenzene, and xylenes) (Moogi et al., 2020; Wang et al., 2020; Zheng et al., 2017; Jung et al., 2010). BTEX compounds are important and valuable products to be recovered from the pyrolysis process that has been reported as the compounds of commercial interest and representing the quality of the pyrolytic oil (Jung et al., 2010; Lopez et al., 2011; Vichaphund et al., 2017). These compounds are widely used in the production of paints and lacquers, adhesives, thinners, inks, rubber products, cosmetics, pharmaceuticals, and other chemical and petrochemical industries (Shafaghat et al., 2018; Gaurh and Pramanik, 2018; Zhang et al., 2019; Wang et al., 2020). Moreover, the lighter fraction hydrocarbons have higher volatility that are suitable for commercial applications as combustion fuels.

The objective of this study was to investigate the application of MSW IBA and IFA as potential low-cost catalysts for *in situ* catalytic reforming of the plastic pyrolysis vapors. The as-received, calcined, and Ni-loaded catalysts were studied in order to evaluate the effect of Ni on product distribution. The change in the leaching behavior of the metals from the ashes before and after the pyrolysis experiments was assessed to study the effect of calcination and pyrolysis processes on the stabilization or destabilization of the heavy metals. A mixture of polypropylene (PP), high density polyethylene (HDPE), and LDPE was utilized as the feedstock in this study as these

plastics represent nearly 50% of all the plastics produced (PlasticsEurope, 2019), thereby forming a significant fraction of the plastic waste stream. The impacts of applying various ashes on the distribution of liquid and gaseous products are reported.

2. Experimental section

2.1. Materials and chemicals

Virgin plastic pellets (2-5 mm) used in the experiments, including PP, HDPE, and LDPE, were purchased from Lotte Chemical Titan Pvt. Ltd., Malaysia. IFA samples including air pollution control (APC) and electrostatic precipitator (ESP) residues were obtained from the Tuas incineration plant, Singapore. The IBA was collected from the Senoko waste to energy incineration plant, Singapore. All the ashes used were aged and have been previously applied in different studies including Yin et al. (2020b; 2021), Chan et al., (2018), and Viet et al., (2020). The chemicals used in the study, including hexane, nitric acid (65% w/w), nickel(II) nitrate, urea, benzene, toluene, ethyl benzene, p-xylene, and o-xylene, were obtained from Sigma Aldrich. Zeolite Socony Mobil-5 (ZSM-5) was purchased from Alfa Aesar.

2.2. Catalyst preparation

Ash samples were homogenized and powdered using a ball mill (Retsch). The milled samples were dried in a hot air oven (105 ℃, 24 h) followed by calcination in a muffle furnace (550 ℃, 2 h). The dried and calcined ash samples were pelletized using a hydraulic press, subsequently crushed, and sieved to a size range of 0.2-2 mm. The samples were denoted as raw (R-) and calcined (C-) ash samples (R-IBA, C-IBA, R-APC, C-APC, R-ESP, and C-ESP). All the samples were stored at 60 ℃ to avoid moisture absorption. The Ni-loaded catalysts were prepared using nickel nitrate that was dissolved in deionized (DI) water. C-APC and urea were then added to the solution with

continuous stirring to obtain a homogenous mixture. The mixture was transferred to a hydrothermal reactor and heated at 120 ℃ for 8 h. Subsequently, the sample was dried at 60 ℃ overnight, ground, calcined (550 ℃, 2 h), and pelletized to the size fraction of 0.2-2 mm. The similar procedure was performed to prepare Ni loaded on ZSM-5 used as a reference catalyst. The catalysts were denoted as 15Ni-APC, 30Ni-APC, and 15Ni-ZSM, where 15 and 30 represent the wt% of Ni loading.

2.3. Plastic pyrolysis and catalytic reforming

The laboratory-scale setup is shown in Figure 1. Plastics (25 g; 70% PP, 24% HDPE, and 6% LDPE) were placed in a customized holder and the catalyst (25 g) was placed in a steel mesh on top of the plastics holder located in a stainless steel batch reactor (inner diameter of 8.3 cm). Upon heating, the primary pyrolysis vapors were reformed while passing through the catalyst bed. N_2 (50 mL/min) (99.995%, Leeden National Oxygen Ltd.) was used as the purge gas for 30 min prior to the heating, the carrier gas, and an internal standard for quantitative gas analysis. In a typical run, the reactor was heated to 500 ℃ (20 ℃/min heating rate) and dwelled for 30 min. The temperature was measured by a thermocouple inserted into the reactor. The mean temperature profile of the experiments is provided in Figure S1. The oil product was collected in a round bottom flask and the non-condensable gas was collected in a gas bag (E-Switch). The mass balance was calculated by weighing the mass of retrieved oil product and calculating the mass of gas product using a known volume of N_2 gas (internal standard). Pyrolysis experiments were conducted in triplicates for all the ash catalysts used and the control study (i.e., experiments without catalyst). The results are reported as mean values of three runs and experimental errors are given as standard deviations. The catalysts were recovered at the end of experiments for subsequent leaching test.

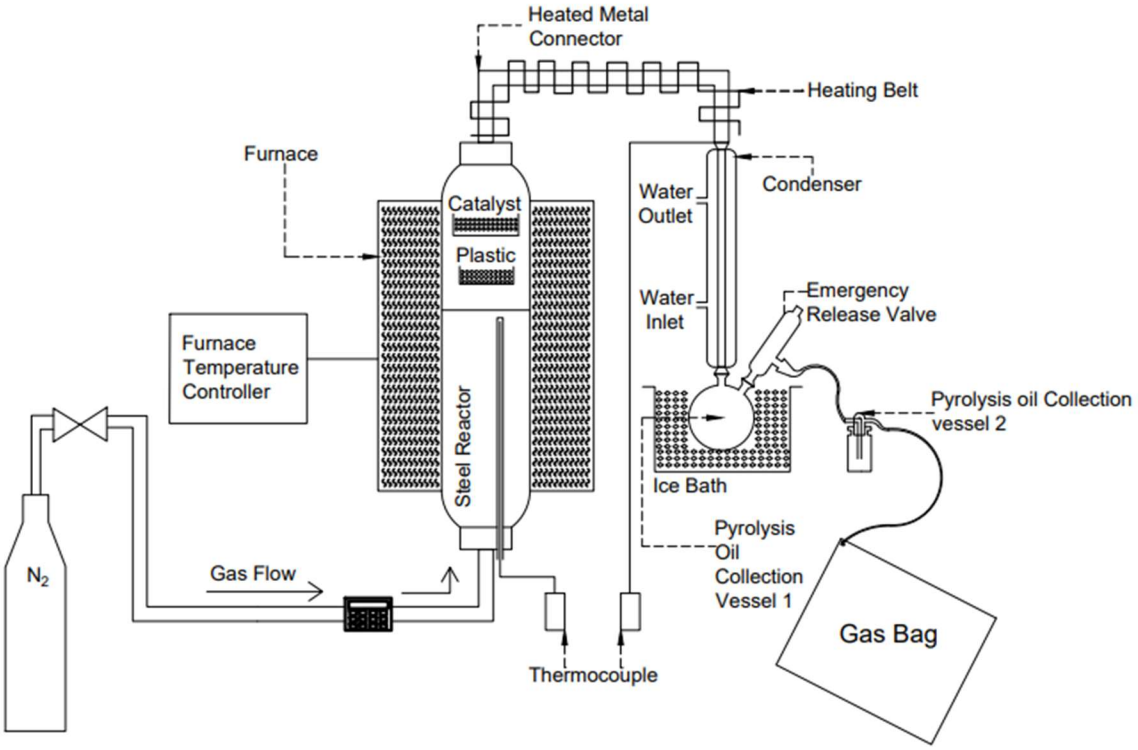

Figure 1. Experimental set up of the plastics pyrolysis and catalytic reforming process.

2.4. Metal leaching

Leaching of metals from the ash catalysts was measured before and after the pyrolysis experiments following the EN 12457-1 standard. 4 g ash sample was mixed with 8 mL DI water at a liquid to solid ratio of 2 L/kg and the mixture was then continuously mixed in an end-over-end tumbler at 30 rpm. After rotating for 24 h, the leachate was collected via vacuum filtration through a 0.45 μm filter paper, subsequently diluted and analyzed using inductively coupled plasma - optical emission spectrometry (ICP-OES, Perkin Elmer Optima 8300) and inductively coupled plasma - mass spectrometry (ICP-MS, Thermo Scientific iCAP Q) for metal contents. The detection limit of the current testing procedure for the elements leached from the ashes was calculated at 0.2 mg/kg.

160 *2.5. Characterization and analytical techniques*

161 Elemental composition of the plastic pellets was measured using CHNS elemental analyzer
162 (Elementar® Vario El Cube). The heating value of the oil product was measured using a bomb
163 calorimeter (IKA C2000 basic). The porosity of ash catalysts was characterized by using
164 Quantachrome Autosorb 1-C, in which the surface area was determined by the Brunauer–Emmett–
165 Teller (BET) method and the total pore volume and average pore diameter were calculated
166 according to the Barret, Joyner, and Halenda method. The X-ray diffraction (XRD) patterns of
167 catalysts were obtained using XRD Bruker D8. Catalyst morphology was characterized using field
168 emission scanning electron microscopy with energy dispersed spectroscopy (FESEM-EDS, JEOL
169 JSM-7600 F). A gas chromatograph coupled with two thermal conductivity detectors and one
170 flame ionization detector (Agilent 7890B) was used to quantify C1-C5 hydrocarbons. The
171 collected gas sample was injected into the gas chromatograph with front detector at 250 °C, split
172 ratio of 80:1, and He as carrier gas. The initial oven program temperature was at 60 °C for 1 min,
173 then increased to 80 °C at 20 °C/min, and further to 190 °C at 30 °C/min and held for 1.33 min
174 (total run time of 7 min). Gas chromatography - mass spectrometry (GC-MS, Agilent 7890B -
175 5977A MSD) was used for the quantitative and qualitative analysis of the oil product. He was used
176 as the carrier gas at the flow rate of 1.2 ml/min and the sample components were separated using
177 Agilent 19091S-433 HP-5MS capillary column (30 m × 0.25 mm × 0.25 μm). 1 μL solution of the
178 oil sample dissolved in hexane was injected into the GC-MS with front inlet at 250 °C and split
179 ratio of 1:1. For the quantitative analysis, the initial oven program temperature was at 30 °C for 3
180 min, then increased to 50 °C at 5 °C/min (held for 2 min), and then ramped up to 300 °C at 20
181 °C/min (total analysis time of 21.5 min). The calibration (5-point calibration, range 0-20 ppm)
182 curve for the quantification of BTEX compounds showed good linearity with R2 values 0.998,

183 0.995, 0.989, 0.994, and 0.995 for benzene, toluene, ethylbenzene, p-xylene, and o-xylene,
184 respectively. Toluene-D8 (D 99.5%, Cambridge Isotope Laboratories, Inc) was used as the internal
185 standard. For the qualitative analysis, the initial oven program temperature was at 30 °C for 3.5
186 min, then increased to 45 °C at 5 °C/min (held for 2 min), then increased to 150 °C at 5 °C/min
187 (held for 2 min), further increased to 175 °C at 5 °C/min (held for 1 min), then ramped up to 220
188 °C at 20 °C/min (held for 1 min), then increased to 265 °C at 5 °C/min (held for 5 min), then
189 increased to 290 °C at 5 °C/min (held for 5 min) and finally ramped up to 320 °C at 20 °C/min
190 (held for 5 min) (total analysis time of 71.25 min). Qualitative analysis revealed the gasoline (C6-
191 C12), diesel (C13-C19), and heavier hydrocarbon (C20-C35) fractions of the oil product. Total
192 metal contents in ash samples were determined by dissolving 0.2 g ash samples in 65% w/w nitric
193 acid via microwave digestion at 200 ℃ for 30 min (Milestone Ethos one). The digested solution
194 was filtered with a syringe filter (PTFE, 0.45 μm). After subsequent dilution using DI water and
195 1.2% HNO_3, samples were analyzed by ICP-OES (quantification limit = 1 mg/L) and ICP-MS
196 (quantification limit = 1 μg/L). After considering the amount of solid samples applied and the
197 dilution required, the detection limit of the current testing procedure for the metal content in ashes
198 was quantified at 2 mg/kg.

199 **3. Results and Discussion**

200 *3.1. Catalytic activity of MSW incineration ashes*

201 According to the CHNS analysis, the plastic mixture contained 86% C, 14% H and traces of N and
202 S (Table S1). The total metal contents of the ashes are reported in Table S3 and were consistent
203 for R-IBA, R-ESP, and R-APC with previous study (Table S2, Lindberg et al., 2015). Figure 2a
204 shows the metal concentrations in the ash samples. Ca, Fe, and Al were the most abundant elements
205 in R-IBA, while Ca, K, and Na had the highest concentrations in both R-ESP and R-APC samples.

Similar to the previous reports (Lam et al., 2010; Yin et al., 2020b), it was observed that the total heavy metal content in R-ESP was higher than R-IBA and R-APC, and several metals in the R-ESP sample (e.g., As, Cd, and Sb) displayed concentrations above 10 times higher than those in R-IBA and R-APC. This phenomenon is likely due to metal vaporization during incineration process as well as metal condensation and adsorption on the surface of fly ash particles (Li et al., 2018). Among the three ashes, R-APC residues had the highest Ca content originating from the addition of slaked lime into the flue gas scrubber for the neutralization of acidic components (Astrup, 2008). In the XRD patterns of R-IBA and C-IBA, crystalline phases of $CaCO_3$, $CaSO_4$, and SiO_2 could be identified (Figure 2b). After calcination, SiO_2 peaks increased possibly due to the formation of crystalline form from amorphous phases, while $CaCO_3$ decreased, possibly due to the partial decomposition of the carbonate and release of CO_2 as supported by the loss on ignition (LOI) observed (Table S4). The XRD patterns of R-ESP and C-ESP revealed the crystalline forms of $CaSO_4$, NaCl, and $K_2Ca(SO_4)_2 \cdot H_2O$. However, insignificant variation in the peaks were observed except the strengthening of the ~26° $CaSO_4$ peak after calcination, indicating that the mineral phases in ESP were stable during calcination. In the XRD patterns of R-APC and C-APC, $CaCO_3$, $CaSO_4$, and CaClOH crystalline phases were observed. The peak of CaClOH became weaker in C-APC while the peak of $CaCO_3$ increased after calcination that may be due to the transformation from CaClOH into $CaCO_3$ via CO_2 reaction (Alfieri et al., 2012; Prigiobbe et al., 2009). The ash samples are inherently complex and was found to be distinctly different from each other. Hence, the variations in the crystalline phases observed via XRD patterns after calcination can be attributed to multiple different reactions, which include the concentration of the compounds due to the loss of organic fractions, reformation from amorphous to crystalline forms,

transformation from one metallic form to another via chemical reactions, and possible carbonation and decarbonation mechanisms.

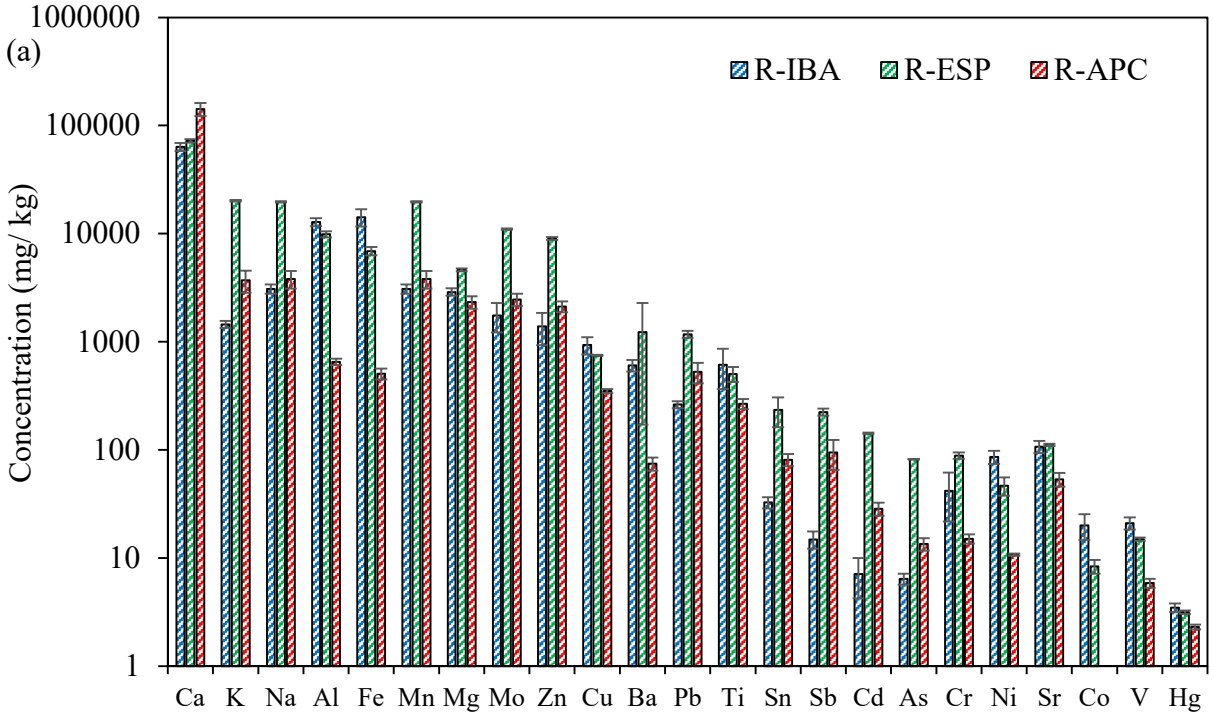

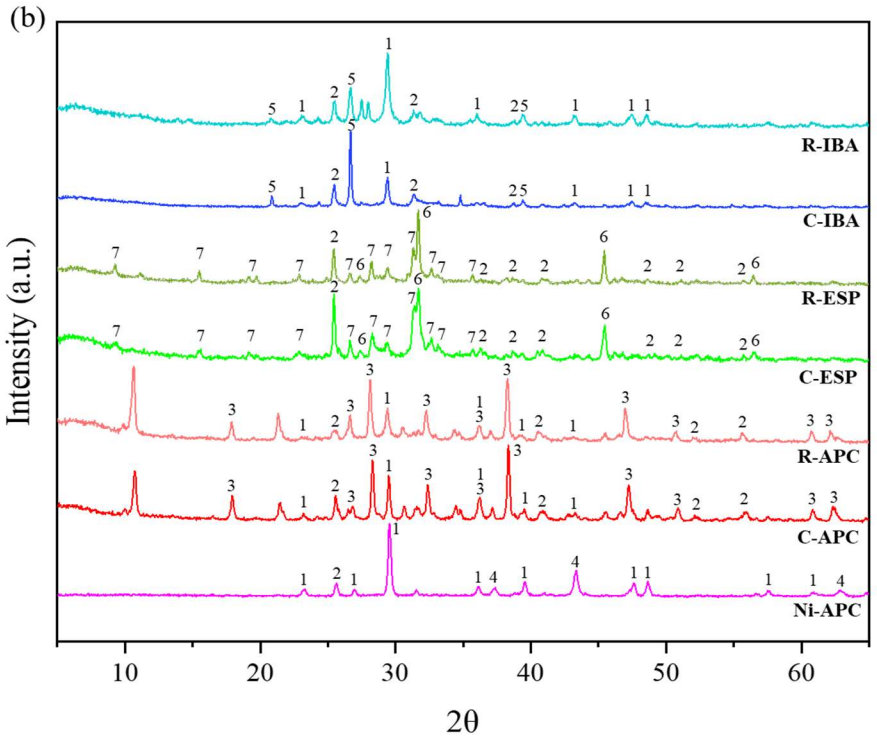

Figure 2. (a) Total metal content in R-IBA, R-ESP and R-APC and (b) XRD patterns of the ash catalysts: 1 – $CaCO_3$, 2 – $CaSO_4$, 3 – CaClOH, 4 – NiO, 5 – SiO_2, 6 – NaCl, 7 – $K_2Ca(SO_4)_2 \cdot H_2O$.

Fig. 3a shows products after in situ catalytic reforming. The oil yield ranged between 76 and 82%, while the gas yield ranged between 13 and 19%. These results were similar to the yields obtained in the control experiment (without the catalyst), suggesting the overall product yield was not affected by the application of the catalysts. No char and ash formation were observed in the pyrolysis experiments due to the usage of virgin polyolefinic plastics, as found in previous studies (Williams & Slaney, 2007; Anene et al., 2018). The mass balance was over 90% for all experiments. The standard deviations were calculated as 4.04, 2.17, 1.64, 3.93, 5.52, 6.86, and 5.70% for control, R-IBA, C-IBA, R-ESP, C-ESP, R-APC, and C-APC catalysts, respectively. There was little variation in calorific value and density among oil samples. The average higher heating value of the pyrolysis oil was 41.7 ± 1.2 MJ/kg, while the density was 0.80 ± 0.03 kg/m^3.

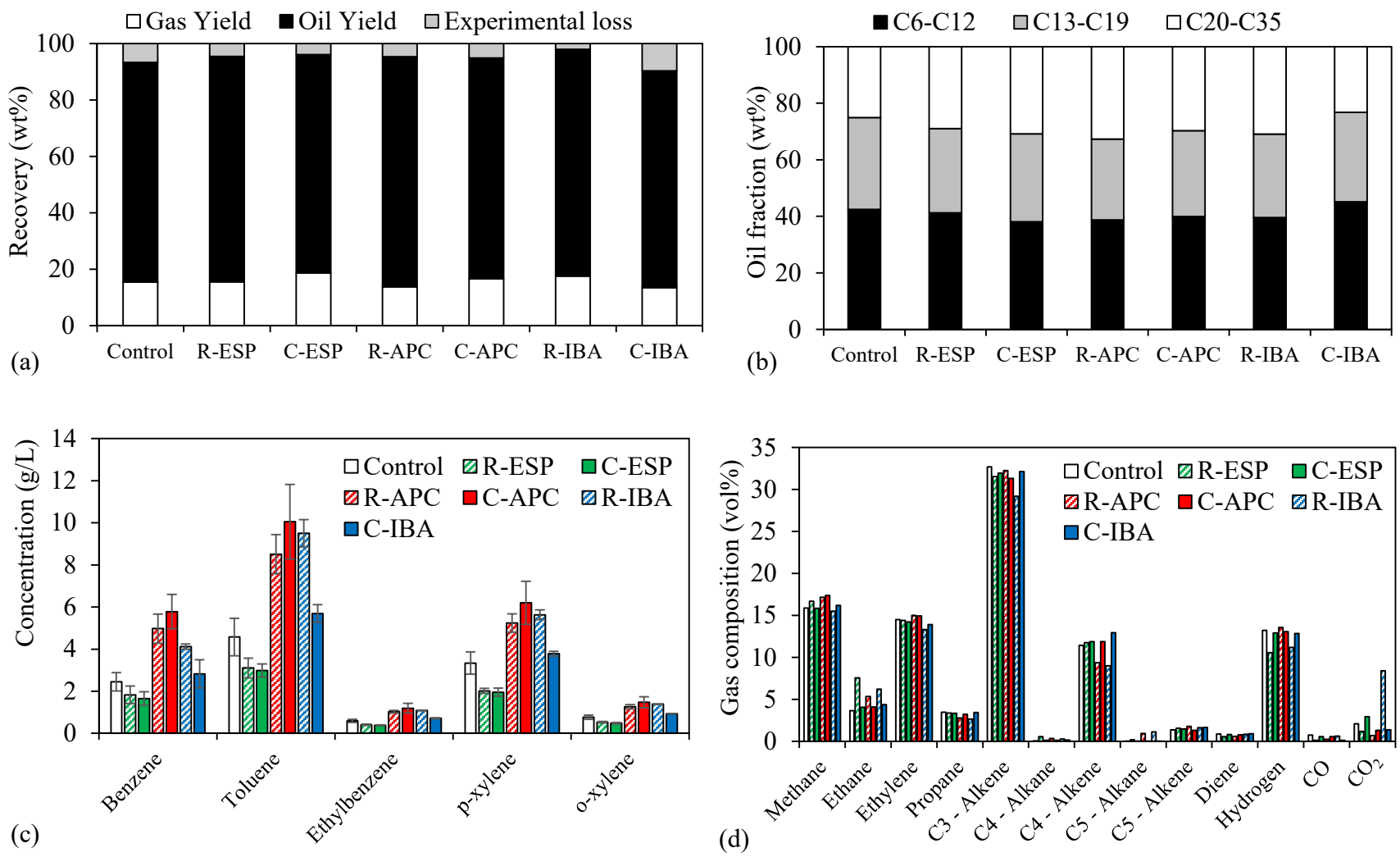

Figure 3. (a) Product yields, (b) qualitative and (c) quantitative assessment results of the pyrolysis oil, and (d) composition of the pyrolysis gas after *in situ* catalytic reforming.

The oil product was characterized qualitatively and quantitatively to determine the fractions of the hydrocarbons. Qualitative analysis revealed the three fractions of hydrocarbons (Veksha et al., 2020), namely, gasoline-like (C6-C12), diesel-like (C13-C19), and heavier hydrocarbon compounds (C20-C35) in the oil product. For the control experiment, on an average 42, 32, and 25% of gasoline-like, diesel-like, and heavier hydrocarbons were observed. Overall, 38-45% gasoline-like, 28-32% diesel-like, and 23-33% heavier hydrocarbon compounds were present in the oil after catalytic reforming using the ash-based catalysts (Figure 3b). Insignificant variation in the distribution of the three compound fractions was observed. After calcination, slight increase was observed in the gasoline-like and diesel-like fractions of the C-IBA and C-APC, while the contrary effect was observed in gasoline-like fraction produced over the C-ESP.

Quantitative analysis of BTEX compounds using GC-MS was conducted to assess the oil product quality (Figure 3c). In comparison to the control experiment, APC and IBA (both raw and calcined) samples resulted in higher concentrations of the BTEX compounds, while ESP resulted in lower yields of these compounds. R-IBA and C-IBA demonstrated considerably increased BTEX yield with R-IBA resulting in the formation of over twice the amount of toluene when compared to the control experiments. According to the metal analysis of ash samples (Figure 2a), Fe is one of the predominant metal species in IBA that may contribute to the catalytic property of IBA residues (Persson et al., 2019; Li et al., 2017). It was reported that Fe-doped zeolite was capable of enhancing monoaromatic hydrocarbons production while inhibiting polyaromatic hydrocarbons formation (Persson et al., 2019). Another study using Fe-pillared clays over pyrolysis of plastic mixture also reported satisfactory catalytic properties with high selectivity towards aromatic compounds (Li et al., 2017). However, the BTEX yield of IBA reduced after calcination possibly due to the crystalline phase transformation and sintering. Compared to the control experiment, the

R-APC produced twice the amount of benzene and 57-86% higher amounts of the other BTEX compounds. The highest yield among all the catalysts was observed for the C-APC producing 136, 120, 102, 86, and 93% higher yield of benzene, toluene, ethylbenzene, p-xylene, and o-xylene, respectively. Calcination was recognized to have positive effect on the BTEX yield of APC, while IBA demonstrated the contrary outcome. This could be attributed to the inherent differences of IBA and APC residues. IBA is the coarse residue that remained after the MSW incineration. The pre-processing applied (crushed and milled) in this study, may expose the active components in this ash (R-IBA), while subsequent calcination could cause transformation and sintering of these components. In contrary, APC is an inherently fine particle residue generated mainly from the slaked lime adsorbing the acidic gases from the flue gas and the particles captured by bag filter. Therefore, the calcination may help to remove the impurities (as supported by LOI analysis) and the conversion of amorphous phases to crystalline phases (as supported by the XRD results). Though qualitative analysis indicated similar performance among the ashes, quantitative analysis revealed the details that may merit the further development of these ashes as catalysts through modification or upgrading.

The gas production results showed insignificant changes between the control experiments and with the use of ash catalysts (Figure 3d). The raw catalysts showed slightly higher ethane yield when compared to the control. The C3-alkenes, including propylene and methyl acetylene, were the dominant among all the gas products. Methane, ethylene, C3-alkenes, C4-alkenes, and hydrogen presented considerable quantities of the gas product. R-IBA showed significantly higher CO_2 due to the possible decarbonation of the carbonates in R-IBA ash releasing CO_2 at elevated temperature (as supported by the 7.4 wt% loss during the LOI analysis).

294 The obtained results confirm that among the three ash samples, APC (and especially, C-APC) has
295 the highest catalytic activity, which is likely attributed to the favorable reformation of its chemical
296 constituents. The major effect of APC as a catalyst is associated with the selective enhancement
297 of BTEX formation. Similarly, the application of calcined coal power plant fly ash produced 1.95
298 to 2.03 times the BTEX contents from waste PE pyrolysis, when compared to the thermal pyrolysis
299 (Gaurh and Pramanik, 2018).

300 *3.2. Metal leaching*

301 One of the major concerns associated with MSW incineration ashes is the leaching of heavy metals
302 into the environment upon disposal (Tucker et al., 2020; Molleda et al., 2020). Since the spent ash
303 catalysts will be disposed or reused in other applications after the loss of catalytic activity, it is
304 necessary to investigate the influence of catalytic reforming on the leaching behavior of heavy
305 metals. The leaching from IBA, APC, and ESP before and after the calcination, and after the
306 pyrolysis experiments was characterized. As shown in Figure 4, metal leaching in all the IBA
307 samples was much lower than that of APC and ESP residues. The trend is comparable to the total
308 metal contents in the three ash residues and is likely attributed to the limited solubility of their
309 metal-containing mineral phases (Yin et al., 2020a). In the case of IBA, the leaching behavior of
310 most elements was consistent before and after both the thermal treatments except for Cr, Mg, and
311 Mo. According to Figure 4a, Cr exhibited significantly increased leaching concentration after
312 calcination but dropped below detection limit after pyrolysis, indicating the facilitating effect of
313 calcination and inhibitory effect of pyrolysis on Cr leaching. The leaching potential of Mg
314 underwent a sharp reduction after both calcination and pyrolysis of R-IBA, revealing the
315 suppressive effect on Mg leachability after heating at elevated temperature of around 500-550 °C.
316 On the contrary, Mo showed increased concentration in leachate after both thermal treatments,

317 suggesting the enhancing effect of high temperature on Mo leaching. Besides, Fe and Al presented
318 low leaching concentrations, in contrast to their high inherent metal contents in IBA residues,
319 indicating the inhibitory effect of metal complexation and/or formation of sparingly soluble metal
320 salts in ash samples (Yin et al., 2020a). Further, by comparing to the European Council Decision
321 (2003/33/EC) for the acceptance of waste at landfills, all the IBA samples were classified under
322 the non-hazardous category and remained in the same category after the calcination and pyrolysis
323 processes.

324 According to Figure 4b, APC released a large amount of alkali metals (K and Na), alkaline earth
325 metal (Ca) as well as Cl^- and SO_4^{2-} anions during leaching, indicating the presence of hydrophilic
326 compounds ($CaCl_2$, $CaSO_4$, KCl, K_2SO_4, NaCl, Na_2SO_4, etc.). Most of the detected elements
327 (except Al, Fe, Mg, Mn, Mo, and Ti) in C-APC exhibited between 20 and 30% incremental
328 leaching as compared with R-APC that may be ascribed to the calcination process decomposing
329 insoluble metallic compounds and thus increasing the metal leachability. After both calcination
330 and pyrolysis of R-APC, Pb exhibited enhanced leaching potential with an increased rate of 78 (C-
331 APC before pyrolysis), 62 (R-APC after pyrolysis), and 73% (C-APC after pyrolysis), indicating
332 that Pb leachability in R-APC is promoted upon thermal treatment. Besides, after calcination, the
333 leaching potential of Fe and Al showed minor decrease (within 20%), while that of Mo and Ti
334 showed slightly higher reduction by 44 and 26%, respectively. After pyrolysis experiments,
335 leaching of most trace elements from APC only showed minor change, apart from enhanced
336 leaching of Ba and Pb from R-APC as well as Zn from C-APC. Overall, Mg and Mn showed lower
337 leachability, while the leaching potential of Pb and Zn increased after calcination and pyrolysis.
338 According to the 2003/33/EC, Pb and Cl^- from all the APC samples exceeded the hazardous
339 criteria. Hg from all the APC samples and Ba from R-APC after pyrolysis exceeded the non-

hazardous criteria. Nevertheless, the overall leaching behavior of the metals in all the APC samples sustained in the same categories as the original sample (R-APC).

C-ESP showed reduced leachability (except for Cr, Mg, Mo, and Pb) after calcination (Figure 4c). One possible cause is that the agglomerated particles formed during the calcination process were less soluble in water (Iretskaya et al., 1999). After the pyrolysis reaction, the leaching of most metals in both R-ESP and C-ESP was enhanced except for Pb, Cr, and Na. Specifically, Cr presented enhanced leaching behavior after calcination but showed decreased leaching potential after pyrolysis. It was deduced that Cr(III) may be oxidized to Cr(VI) during the calcination process forming soluble compounds that were responsible for the increased Cr leachability (Zhu et al., 2018). In contrast, the suppression of Cr leaching after pyrolysis may be due to the complexation with copper and calcium that could immobilize Cr (Zhou et al., 2018). Further, according to the 2003/33/EC, leaching of Cl^- slightly exceeded (or around the borderline) the hazardous waste criteria in R-ESP (16873 ± 214 mg/kg) and C-ESP (17021 ± 203 mg/kg) samples after the pyrolysis experiment. Mo in all the four ESP and Cr in C-ESP (before) samples exceeded leaching limits of the non-hazardous criteria. Therefore, all the ESP samples were classified under the non-hazardous category and remained in the same category after the calcination and pyrolysis processes except for the Cl^- anions.

Overall, minimal changes to the metal leaching potentials were observed except for the reduced leaching of Mg and increased leaching of Mo in IBA after both thermal processes; reduced leaching of Mg and Mn, and increased leaching of Pb and Zn in APC after both thermal processes; and enhanced leaching after calcination and reduced leaching after pyrolysis for Cr in ESP samples. Generally, the use of ashes in catalytic reforming application caused minimal deterioration to their leaching behavior and all ashes remained in the same category as classified

363 based on 2003/33/EC except Cl^- from the ESP, which can be addressed by a simple washing
364 process, if necessary. Nevertheless, as the ESP samples (with or without calcination) demonstrated
365 very low potential to be used as the catalysts for reforming plastic pyrolysis vapor, it is
366 recommended to avoid the pyrolytic treatment of this ash.

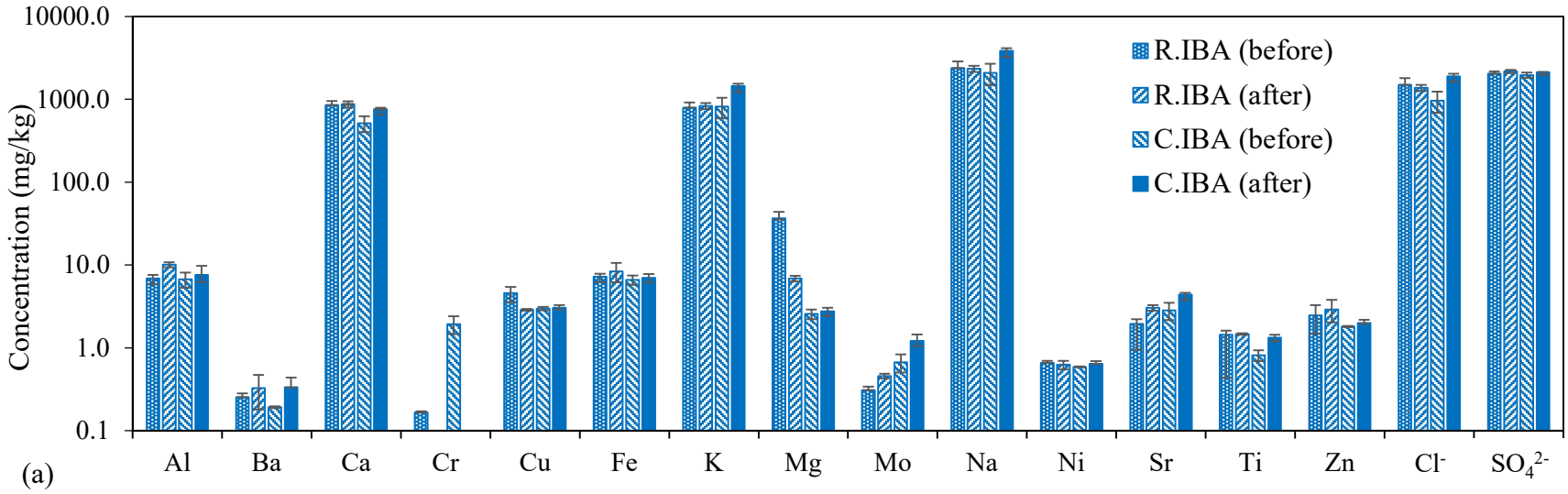
10000.0
1000.0
100.0
10.0
1.0
0.1
Concentration (mg/kg)
R.IBA (before)
R.IBA (after)
C.IBA (before)
C.IBA (after)
Al
Ba
Ca
Cr
Cu
Fe
K
Mg
Mo
Na
Ni
Sr
Ti
Zn
Cl-
SO4 2-

(a)

367

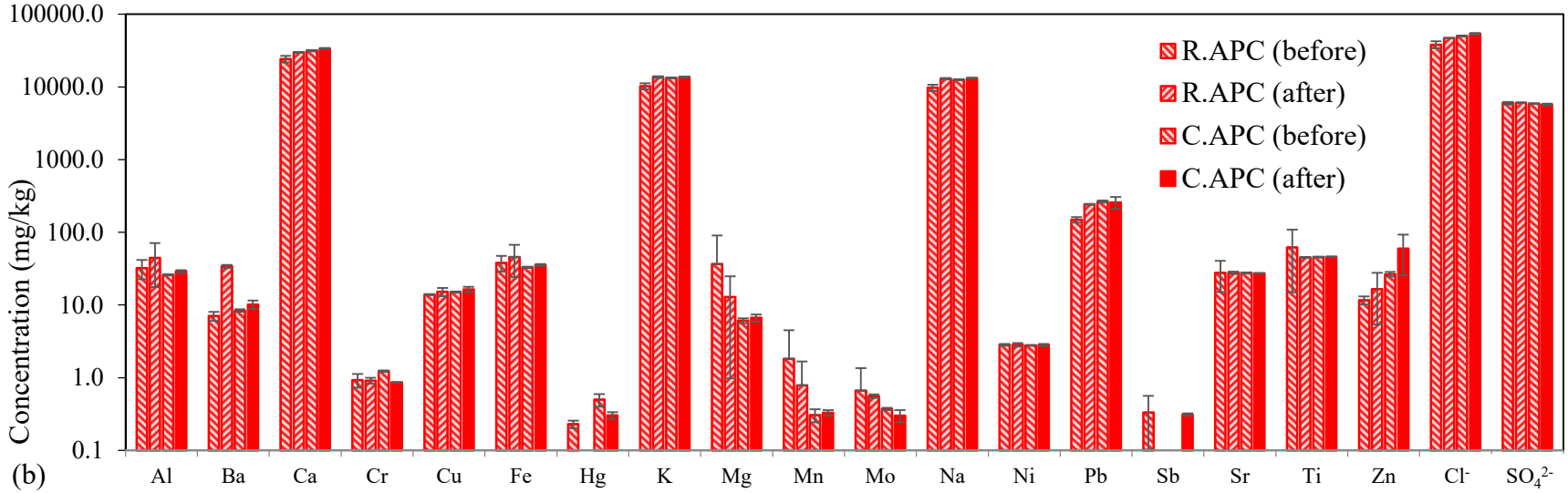
100000.0
10000.0
1000.0
100.0
10.0
1.0
0.1
Concentration (mg/kg)
R.APC (before)
R.APC (after)
C.APC (before)
C.APC (after)
Al
Ba
Ca
Cr
Cu
Fe
Hg
K
Mg
Mn
Mo
Na
Ni
Pb
Sb
Sr
Ti
Zn
Cl-
SO4 2-

(b)

368

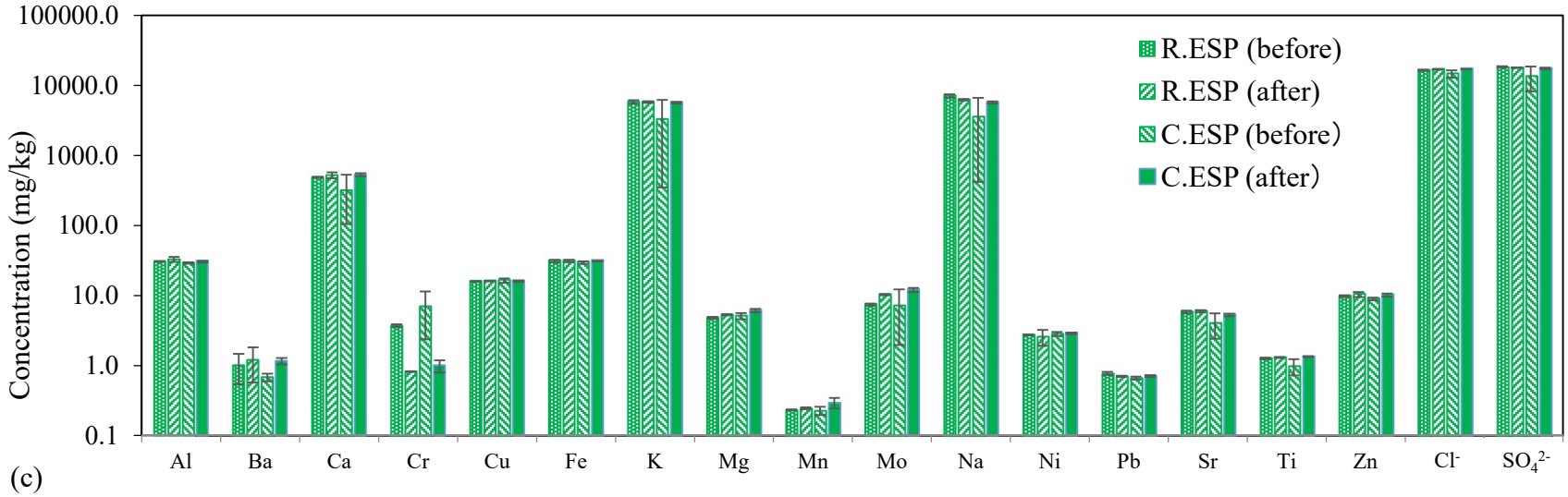

(c)

Figure 4. Concentrations of leaching elements in (a) R-IBA and C-IBA, (b) R-APC and C-APC, and (c) R-ESP and C-ESP before and after pyrolysis experiments.

372 *3.3. Effect of Ni loading on C-APC*

373 Owing to its superior catalytic activity compared to the other ash samples, C-APC was loaded with
374 Ni to further investigate the effect of using the ash on oil and gas production. The differences
375 between Ni supported on C-APC and ZSM were investigated and compared, as the ZSM based
376 catalysts are widely used for oil reforming (Miandad et al., 2016; Yao et al., 2018; Miskolczi et
377 al., 2019). BET results revealed that upon hydrothermal treatment and Ni loading of the C-APC
378 catalyst, the surface area, pore volume, and pore diameter increased (Table 1). However, the
379 porous characteristics of 15Ni-APC remained lower compared to the 15Ni-ZSM.

380 Table 1. Porous properties of C-APC, 15Ni-APC, and 15Ni-ZSM catalysts.

Catalyst	BET surface area (m^2/g)	Total pore volume (cm^3/g)	Average pore diameter (nm)
C-APC	1.5	0.003	18.3
15Ni-APC	5.6	0.018	64.7
15Ni-ZSM	267	0.130	16.4

381

382 The XRD pattern of 15Ni-APC is shown in Figure 2b. NiO peaks were identified in 15Ni-APC
383 indicating the successful impregnation of nickel. The peak of CaClOH disappeared in 15Ni-APC,
384 while the peak of $CaCO_3$ strengthened showing the prevalence of the $CaCO_3$ crystalline phase.
385 FESEM-EDS analysis depicting the surface morphology and Ni content in R-APC, C-APC, 15Ni-
386 APC, and 15Ni-ZSM catalysts is shown in Figure 5 and Figure S3. The 15Ni-ZSM particle sizes
387 ranged between 200-500 nm, while the APC ash samples demonstrated greater heterogeneity

388 including the presence of agglomerated structures. The even distribution of Ni in 15Ni-APC and
389 15Ni-ZSM was confirmed by the FESEM-EDS mapping.

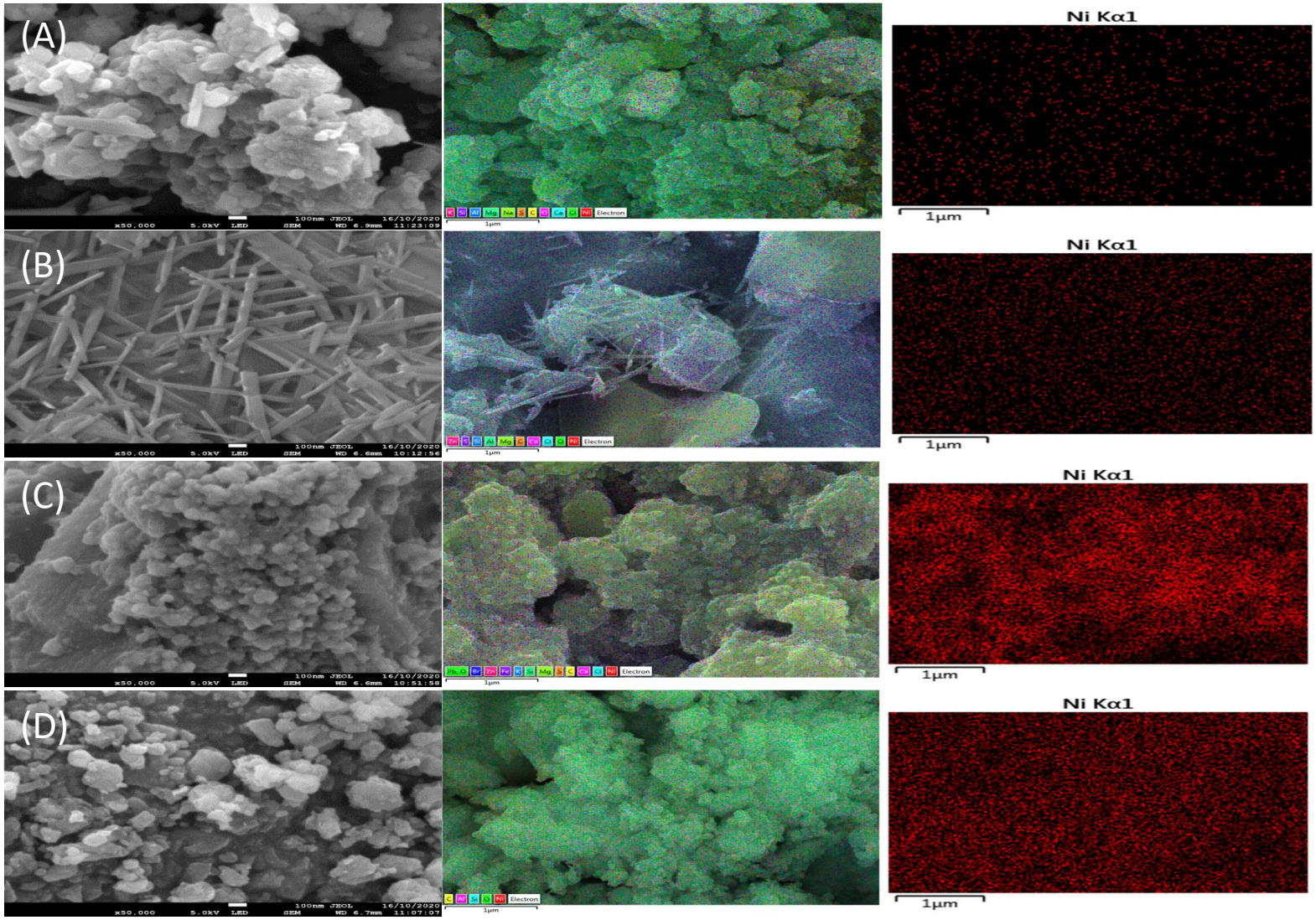

Figure 5. FESEM-EDS micrographs of the (A) R-APC, (B) C-APC, (C) 15Ni-APC, and (D) 15Ni-ZSM catalysts depicting the crystalline structures and Ni distribution.

393 The use of Ni-APC catalysts resulted in significantly higher oil fraction (85-90%) and reduced gas
394 fraction (4-10%) when compared to 15Ni-ZSM (Oil: 77%; Gas: 17%) (Figure 6a). A similar effect
395 was observed with clay that was attributed to its mild acidity (Gobin & Manos, 2004). The decrease
396 in oil fraction of 15Ni-ZSM could be attributed to the overcracking of the primary pyrolysis
397 products by the zeolite because of its mesoporous structure with high BET surface and acidity (Seo
398 et al., 2003; Miandad et al., 2017; Sebestyén et al., 2017).

399 Increasing the Ni content of the Ni-APC from 15 to 30% resulted in a further increase in the heavier
400 hydrocarbon contents (Figure 6b), which is attributable to the increase in the pore size when
401 compared to C-APC. Among all the samples, the lowest gasoline-like (30%) and highest heavier
402 hydrocarbon (40%) fractions were observed for the 30Ni-APC catalyst. Similar observation was
403 reported by Lopez et al. (2011), who observed the higher amounts of heavier hydrocarbons
404 obtained for Al-MCM-41 catalysts as compared to HZSM-5 due to the large pore size and lower
405 acidity of Al-MCM-41. This could explain the significant increase of heavier hydrocarbon
406 fractions over Ni-APCs as well. On the other hand, 15Ni-ZSM demonstrated a significantly higher
407 gasoline-like fraction of 67%, while the diesel-like and heavier hydrocarbon fractions were 19 and
408 14%, respectively.

409 Ni-APCs and C-APC demonstrated inferior BTEX yield when compared to 15Ni-ZSM. The BTEX
410 formation of 15Ni-ZSM was 64, 34, 306, 201, and 301% greater for benzene, toluene,
411 ethylbenzene, p-xylene, and o-xylene compounds, respectively, when compared to C-APC (Figure
412 6c). The metal loading of the zeolites has been reported to increase the BTEX formation
413 (Iliopoulou et al., 2012; Vichaphund et al., 2017). The Ni-APCs yielded lower BTEX content than
414 the 15Ni-ZSM and C-APC, possibly due to the greater pore size of the Ni-APCs. This is because
415 the heavier hydrocarbon compounds are favored by the larger pores of Ni-APCs, while smaller

pore size favored lighter hydrocarbons when compared to the control (Figure S2). Therefore, it can be concluded that the use of Ni loaded APC can promote the production of pyrolysis oil but with increased heavier hydrocarbons and reduced BTEX in the oil.

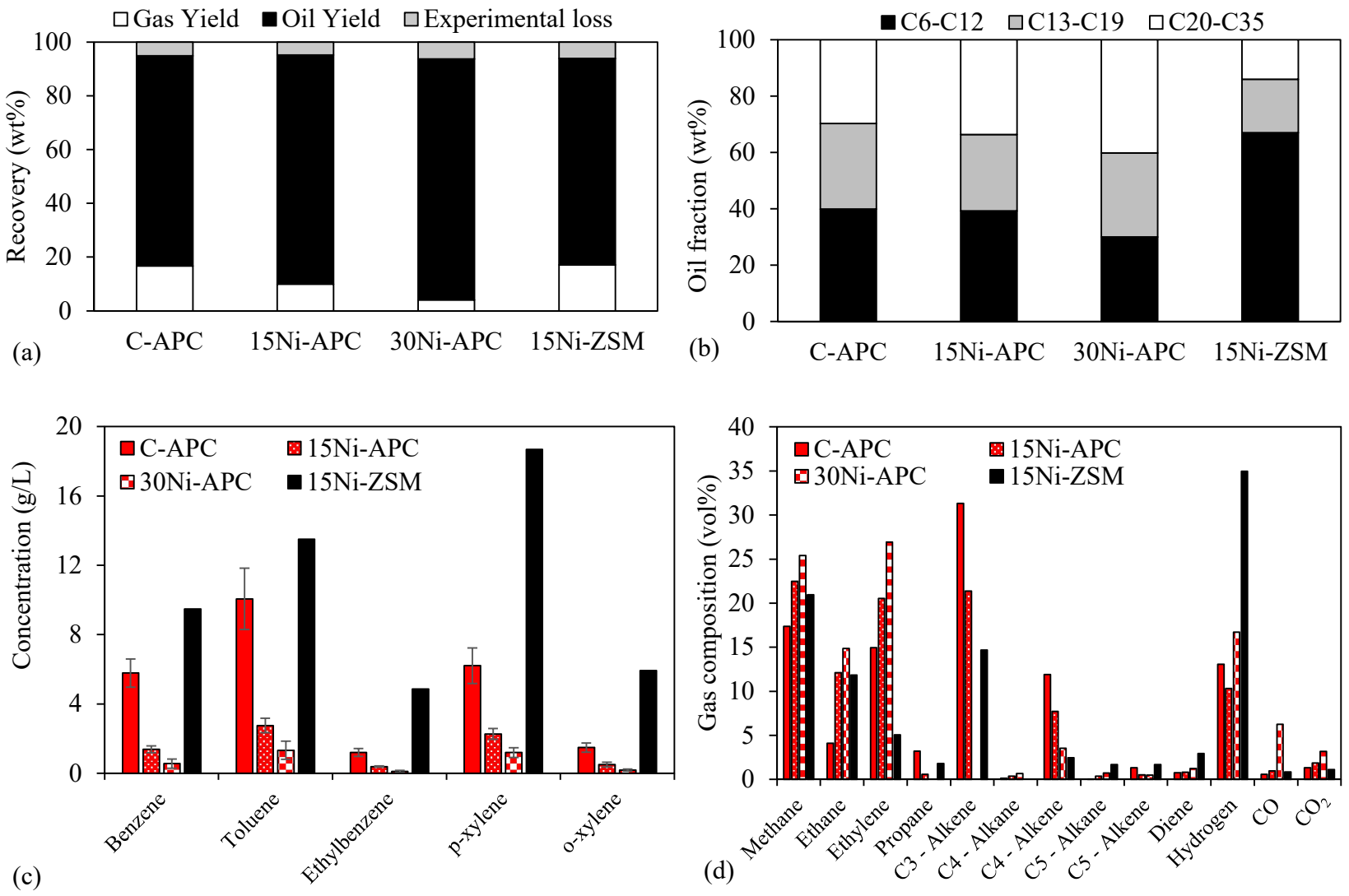

Figure 6. (a) Product yields, (b) qualitative and (c) quantitative assessment results of the pyrolysis oil product, and (d) composition of the pyrolysis gas product in the *in situ* catalytic reforming of plastic pyrolysis vapors with various Ni loaded catalysts.

423 The compositions of the gas products for the Ni loaded catalyst samples and C-APC were found
424 to be different (Figure 6d). A significant increase of methane (29 and 46%), ethane (195 and
425 262%), and ethylene (37 and 80%) was observed for 15Ni-APC and 30Ni-APC, respectively, when
426 compared to the C-APC. Concurrently, C3-alkenes reduced by 32 and 100%, and C4-alkenes
427 reduced by 35 and 70% for 15Ni-APC and 30Ni-APC, respectively. Similarly, an increase of 21,
428 189, and 167% in methane, ethane, and hydrogen, respectively, was observed for the 15Ni-ZSM
429 when compared to the C-APC catalyst. On the other hand, a simultaneous reduction was observed
430 for ethylene (66%), C3- (53%), and C4-alkenes (79%) indicating the catalytic conversion of the
431 alkenes into shorter chain alkanes and hydrogen. The observed trend demonstrated the potential
432 influences of the Ni-loaded ash catalysts on the pyrolysis gas products. In summary, Ni loaded
433 APC showed greater yield of methane, ethane, and ethylene, but lower H_2 as compared to the Ni-
434 ZSM. The formation of short-chain gaseous hydrocarbons and hydrogen were favored by the Ni
435 loaded catalysts, while the simultaneous reduction of C3- and C4-alkenes were observed.

436 *3.4. Limitations and future research recommendations*

437 This study showed that APC and IBA are potentially useful for catalytic reforming of plastic
438 pyrolysis vapors for oil and gas production. The application of ash is appealing because of its
439 origin from a waste source. The reuse of waste resources for productive applications will contribute
440 towards circularity of resource use and achieving the sustainable development goal of 'responsible
441 consumption and production' set by the United Nations. Although the oil quality from ash is
442 inferior to Ni-ZSM, further post-treatment, including distillation or refining, can be applied to
443 facilitate the commercial application of the pyrolysis oil and gas. Some commercial applications
444 include, blending different fractions of pyrolysis oil with conventional diesel to operate diesel

engines (Nileshkumar et al., 2015; Panda et al., 2016) and separation of propylene and ethane from pyrolysis gas to be used as a chemical feedstock for polyolefin production (Sharuddin et al., 2016).

There are few limitations in this study. Firstly, the plastics used for these experiments were virgin plastics, which are generally cleaner, with no generation of char residue and acidic gases. Hence, further research is required to evaluate the effects of mixed waste plastics on the ash catalysts when compared to the commercial catalyst and establish the operating conditions, catalytic activity, and product yields. Although this study demonstrated the positive effect of ash as a catalyst, it fails to reflect how charring (or coking) can affect the catalytic and leaching performances of the ashes. For instance, in the case of waste plastics, due to the presence of fillers in the plastic products the residual ash content can be up to 26% of the initial weight (Ahamed et al., 2021) that can amplify the charring. Coke deposition over the surface of the catalysts leading to the rapid deactivation of the catalysts has been reported as a barrier to the effective usage of the commercial catalysts (Moogi et al., 2020; Lee et al., 2016; Shafaghat et al., 2018). On the other hand, effects of coking on the ashes may diminish their leaching potential. For instance, the biochar from sewage sludge pyrolysis was reported to exhibit reduced leaching characteristics owing to the conversion of heavy metals to a more stable form (Dou et al., 2017; Udayanga et al., 2018; 2019). In the case of using incineration ash in catalytic pyrolysis, the coke deposition on the surface of the spent catalyst could be beneficial as a stabilization method for the ashes and facilitate in the subsequent application in land reclamation and construction sectors. This could potentially offset the need for waste management (landfill) of the incineration ashes.

Secondly, when preparing the ash catalysts, the optimal pretreatment including size fractionation, acid treatment, and calcination temperatures should be investigated. The relatively poor catalytic selectivity of R-APC, C-APC, and Ni-APC may be correlated with their lower surface area and

higher average pore diameter when compared to Ni-ZSM (Table 1). An effective pretreatment will be capable of removing the possible impurities and enhancing physicochemical properties of catalysts with regard to the surface area and pore volume. For example, Gaurh and Pramanik (2018) prepared coal power plant fly ash catalysts for waste PE pyrolysis using various calcination temperatures. The fly ash calcined at 800 ℃ was found possessing the highest surface area, pore volume, and Si/Al ratio, resulting in significantly improved oil quality with elevated BTEX concentration. Nevertheless, it was also demonstrated that further increase of temperature might lead to contradictory results such as much lower surface area and oil quality, indicating the importance of selecting an optimized calcination temperature.

Thirdly, incorporation of other types of heteroatoms, especially metal species, into the pretreated ash framework can be a feasible way to enhance the catalytic performance of ashes, owing to their ability to increase acidic strength and amount of Lewis acid sites of catalysts (Aguado et al., 2008; Li et al., 2017). For example, Ga impregnated ZSM-5 displayed superior selectivity towards aromatic hydrocarbons owing to enriched Lewis acid sites and stronger acidic strength (Xin et al., 2019). Besides, Co, Ni, Zn, and Fe modified HZSM-5 catalysts were also reported to exhibit enhanced catalytic activity that contributed to higher oil yield and quality (Razzaq et al., 2019). Hence, more metal modifications on ash catalysts could be implemented in subsequent studies for the purpose of achieving desired catalytic activity.

In addition, catalyst/feedstock ratio (1/1 wt%) needs to be optimized in future studies. Studies with zeolite-based catalyst have reported catalyst/feedstock ratio of 1/10 (Anene et al., 2018; Miandad et al., 2017). It is important to note that a low ratio may lead to insufficient surface contact time while a ratio exceeding the proper range with relatively longer contact time may accelerate coke formation followed by the deactivation of the active sites (Kantarelis et al., 2014). Moreover, the

491 successful application of incineration ashes would yield a possible double benefit by serving the
492 plastic pyrolysis process and facilitating a possible treatment and beneficial application of the
493 incineration ashes.

494 Pyrolysis has various operational and environmental advantages including lower carbon footprint
495 over combustion and gasification (Al-Salem et al., 2017; Qureshi et al., 2020; Das et al., 2021).
496 However, the use of zeolite was reported to cause significant impact on the environment including
497 climate change and toxicity potentials and was concluded as one of the environmental hotspots of
498 the plastic pyrolysis process (Ahamed et al., 2020). Successful substitution of the zeolite with
499 incineration ash residue can alleviate the environmental footprint of the zeolite application in
500 pyrolysis processes. Hence, this research provides a novel option to further improve the
501 environmental footprint of the catalytic reforming of the plastic pyrolysis process. Further, this
502 research also provides avenue for diverting the incineration ashes from landfilling and reuse in
503 beneficial applications that encourages the concepts of circular economy and sustainable
504 development.

505 **4. Conclusion**

506 In conclusion, the use of MSW IBA and APC promoted selective production of BTEX compounds
507 for in-line upgrading of volatile plastic pyrolysis products when compared to the control
508 experiments, while ESP lowered BTEX formation. Calcination of APC (C-APC) further improved
509 the BTEX yield. Further, the influence of pyrolysis and calcination on the ash catalysts caused
510 minimal changes to the leaching of metals. Comparison of the leaching limit values stated in the
511 European Council Decision 2003/33/EC for the acceptance of hazardous waste at landfills
512 determined that all the ashes applied generally remained in the same category after the calcination
513 and pyrolysis processes, except for the leaching of Cl^- from the ESP. Therefore, the use of ashes

514 in catalytic reforming application do not significantly deteriorate their leaching behavior. In the
515 case of Ni-loaded catalysts, the Ni-APCs resulted in increase of the overall oil fraction and reduced
516 gas fraction when compared to the benchmark Ni-ZSM catalyst. However, lower gasoline-like
517 fraction and BTEX compounds were observed for Ni-APCs when compared to C-APC and Ni-
518 ZSM. In the case of gas products, the formation of short-chain hydrocarbons and hydrogen were
519 favored by the Ni loaded catalysts, while the simultaneous reduction of C3- and C4-alkenes was
520 observed. This study reports a preliminary investigation of the application of ash in catalytic
521 reforming and demonstrates its potential. Therefore, the development of the ash catalysts through
522 pre-treatments including size fractionation, acid treatment, refining, and modifications, and
523 subsequent optimization can be beneficial to realize the true potential in catalytic reforming of
524 plastic pyrolysis vapor. Additionally, coke deposition on the catalyst may be explored as an
525 immobilization method for the heavy metals in the ashes in the future studies. This study also
526 provides an avenue for testing ashes in various catalytic applications. Successful replacement of
527 the reliance on natural/synthetic catalysts with waste-derived catalyst developed from residual ash
528 could incur significant environmental and economic benefits.

529 **Declaration of competing interest**

530 The authors declare no competing interests.

531 **CRediT authorship contribution statement**

532 **Ashiq Ahamed:** Conceptualization; Methodology; Experimental investigation; Materials
533 characterization; Data analysis; Writing - original draft; Writing - review & editing. **Lili Liang:**
534 Experimental investigation; Materials characterization; Data analysis; Writing - original draft. **Wei**
535 **Ping Chan:** Methodology; Experimental investigation; Materials characterization; Data analysis;

Writing - review & editing. **Preston Choon Kiat Tan:** Experimental investigation; Materials characterization. **Nicklaus Tze Xuan Yip:** Experimental investigation; Materials characterization. **Andrei Veksha:** Methodology; Supervision; Writing - review & editing. **Ke Yin:** Conceptualization; Writing - review & editing. **Johan Bobacka:** Writing - review & editing. **Grzegorz Lisak:** Supervision; Conceptualization; Project administration; Funding acquisition; Resources; Writing - review & editing.

Acknowledgement

The authors would like to acknowledge the Nanyang Environment and Water Research Institute, Nanyang Technological University (Singapore), and Economic Development Board (Singapore) for the financial support of this research.

References

1. Aguado, J., Serrano, D.P., Escola, J.M., 2008. Fuels from Waste Plastics by Thermal and Catalytic Processes: A Review. Ind. Eng. Chem. Res. 47, 7982-7992.
2. Ahamed, A., Vallam, P., Iyer, N.S., Veksha, A., Bobacka, J., Lisak, G., 2021. Life cycle assessment of plastic grocery bags and their alternatives in cities with confined waste management structure: A Singapore case study. J. Clean. Prod. 278, 123956.
3. Ahamed, A., Veksha, A., Yin, K., Weerachanchai, P., Giannis, A., Lisak, G., 2020. Environmental impact assessment of converting flexible packaging plastic waste to pyrolysis oil and multi-walled carbon nanotubes. J. Hazard. Mater. 390, 121449.
4. Al-Rahbi, A.S., Williams, P.T., 2019. Waste ashes as catalysts for the pyrolysis–catalytic steam reforming of biomass for hydrogen-rich gas production. J. Mater. Cycles Waste. 21, 1224–1231.

5. Al-Salem, S., Antelava, A., Constantinou, A., Manos, G., Dutta, A., 2017. A review on thermal and catalytic pyrolysis of plastic solid waste (PSW). J. Environ. Manage. 197, 177–198.
6. Alfieri, F., Gunning, P., Gallo, M., Del Borghi, A., Hills, C., 2012. Monitoring of carbon dioxide uptake in accelerated carbonation processes applied to air pollution control residues. Proceedings of Ecos 2012 - The 25th International Conference on Efficiency, Cost, Optimization, Simulation and Environmental Impact of Energy Systems.
7. Anene, A.F., Fredriksen, S.B., Sætre, K.A., Tokheim, L.-A., 2018. Experimental Study of Thermal and Catalytic Pyrolysis of Plastic Waste Components. Sustainability 10, 3979.
8. Ashok, J., Das, S., Yeo, T.Y., Dewangan, N., Kawi, S., 2018. Incinerator bottom ash derived from municipal solid waste as a potential catalytic support for biomass tar reforming. Waste Manage. 82, 249–257.
9. Astrup, T., 2008. Management of APC residues from W-t-E plants. An overview of management options and treatment methods. ISWA General Secretariat, Copenhagen, Denmark.
10. Auxilio, A., Choo, W., Kohli, I., Chakravartula Srivatsa, S., Bhattacharya, S., 2017. An experimental study on thermo-catalytic pyrolysis of plastic waste using a continuous pyrolyser. Waste Manage. 67, 143–154.
11. Chan, W.-P., Ren, F., Dou, X., Yin, K., Chang, V.W.-C., 2018. A large-scale field trial experiment to derive effective release of heavy metals from incineration bottom ashes during construction in land reclamation. Sci. Total Environ. 637–638, 182-190.
12. Cudjoe, D., Acquah, P.M., 2021. Environmental impact analysis of municipal solid waste incineration in African countries. Chemosphere 265 (2021) 129186.

581 13. Das, P., Gabriel, J.-C.P., Tay, C.Y., Lee, J.-M., 2021. Value-added products from
582 thermochemical treatments of contaminated e-waste plastics. Chemosphere 269 (2021)
583 129409.
584 14. Dou, X., Chen, D., Hu, Y., Feng, Y., Dai, X., 2017. Carbonization of heavy metal
585 impregnated sewage sludge oriented towards potential co-disposal. J. Hazard. Mater. 321,
586 132–145.
587 15. Dou, X., Ren, F., Nguyen, M.Q., Ahamed, A., Yin, K., Chan, W.P., Chang, V.W.-C., 2017.
588 Review of MSWI bottom ash utilization from perspectives of collective characterization,
589 treatment and existing application. Renew. Sust. Energ. Rev. 79, 24–38.
590 16. European Council Decision, 2003/33/EC. The Council of the European Union, Official
591 Journal of the European Communities, L 11, 27-49.
592 17. Gaurh, P., Pramanik, H., 2018. Production of benzene/toluene/ethyl benzene/xylene (BTEX)
593 via multiphase catalytic pyrolysis of hazardous waste polyethylene using low cost fly ash
594 synthesized natural catalyst. Waste Manage. 77, 114-130.
595 18. Gobin, K., Manos, G., 2004. Polymer degradation to fuels over microporous catalysts as a
596 novel tertiary plastic recycling method. Polym. Degrad. Stabil. 83, 267-279.
597 19. Huang, Q., Lu, P., Hu, B., Chi, Y., Yan, J., 2016. Cracking of Model Tar Species from the
598 Gasification of Municipal Solid Waste Using Commercial and Waste-Derived Catalysts.
599 Energ. Fuel. 30, 5740−5748
600 20. Iliopoulou, E., Stefanidis, S., Kalogiannis, K., Delimitis, A., Lappas, A., Triantafyllidis, K.,
601 2012. Catalytic upgrading of biomass pyrolysis vapors using transition metal-modified ZSM-
602 5 zeolite. Appl. Catal. B-Environ. 127, 281–290.

603 21. Iretskaya, S., Nzihou, A., Zahraoui, C., Sharrock, P., 1999. Metal leaching from MSW fly
604 ash before and after chemical and thermal treatments. Environ. Prog. 18, 144-148.
605 22. Jung, S.-H., Cho, M.-H., Kang, B.-S., Kim, J.-S., 2010. Pyrolysis of a fraction of waste
606 polypropylene and polyethylene for the recovery of BTX aromatics using a fluidized bed
607 reactor. Fuel Process. Technol. 91, 277–284.
608 23. Kantarelis, E., Yang, W., Blasiak, W., 2014. Effect of zeolite to binder ratio on product
609 yields and composition during catalytic steam pyrolysis of biomass over transition metal
610 modified HZSM5. Fuel 122, 119-125.
611 24. Lam, C. H., Ip, A. W., Barford, J. P., McKay, G., 2010. Use of incineration MSW ash: a
612 review. Sustainability 2, 1943-1968.
613 25. Lee, H., Kim, Y.-M., Lee, I.-G., Jeon, J.-K., Jung, S.-C., Chung, J.D., Choi, W.G., Park, Y.-
614 K., 2016. Recent advances in the catalytic hydrodeoxygenation of bio-oil. Korean J. Chem.
615 Eng. 33, 3299–3315.
616 26. Lei, Z., Hao, S., Yang, J., Zhang, L., Fang, B., Wei, K., Lingbo, Q., Jin, S., Wei, C., 2020.
617 Study on denitration and sulfur removal performance of Mn-Ce supported fly ash catalyst.
618 Chemosphere (In Press) 128646. https://doi.org/10.1016/j.chemosphere.2020.128646
619 27. Li, K., Lei, J., Yuan, G., Weerachanchai, P., Wang, J.-Y., Zhao, J., Yang, Y., 2017. Fe-, Ti-,
620 Zr- and Al-pillared clays for efficient catalytic pyrolysis of mixed plastics. Chem. Eng. J.
621 317, 800-809.
622 28. Li, W., Ma, Z., Huang, Q., Jiang, X., 2018. Distribution and leaching characteristics of heavy
623 metals in a hazardous waste incinerator. Fuel 233, 427-441.
624 29. Lindberg, D., Molin, C., Hupa, M., 2015. Thermal treatment of solid residues from WtE
625 units: A review. Waste Manage. 37, 82-94.

626 30. Lopez, A., de Marco, I., Caballero, B.M., Laresgoiti, M.F., Adrados, A., Aranzabal, A., 2011.
627 Catalytic pyrolysis of plastic wastes with two different types of catalysts: ZSM-5 zeolite and
628 Red Mud. Appl. Catal. B Environ. 104, 211–219.
629 31. Miandad, R., Barakat, M., Aburiazaiza, A., Rehan, M., Nizami, A., 2016. Catalytic pyrolysis
630 of plastic waste: A review. Process Saf. Environ. 102, 822–838.
631 32. Miandad, R., Barakat, M., Rehan, M., Aburiazaiza, A., Ismail, I., Nizami, A., 2017. Plastic
632 waste to liquid oil through catalytic pyrolysis using natural and synthetic zeolite catalysts.
633 Waste Manage. 69, 66–78.
634 33. Miskolczi, N., Juzsakova, T., Sója, J., 2019. Preparation and application of metal loaded
635 ZSM-5 and y-zeolite catalysts for thermo-catalytic pyrolysis of real end of life vehicle
636 plastics waste. J. Energy Inst. 92(1), 118–127.
637 34. Molleda, A., Lopez, A., Cuartas, M., Lobo, A., 2020. Release of pollutants in MBT landfills:
638 Laboratory versus field. Chemosphere 249 (2020) 126145.
639 35. Moogi, S., Jae, J., Kannapu, H.P.R., Ahmed, A., Park, E.D., Park, Y.-K., 2020. Enhancement
640 of aromatics from catalytic pyrolysis of yellow poplar: Role of hydrogen and methane
641 decomposition. Bioresource Technol. 315, 123835.
642 36. Na, J.-G., Jeong, B.-H., Chung, S.H., Kim, S.-S., 2006. Pyrolysis of low-density
643 polyethylene using synthetic catalysts produced from fly ash. J. Mater. Cycles Waste. 8, 126–
644 132.
645 37. Nileshkumar, K.D., Jani, R.J., Patel, T.M., Rathod, G.P., 2015. Effect of blend ratio of plastic
646 pyrolysis oil and diesel fuel on the performance of single cylinder CI engine. Int. J. Sci.
647 Technol. Eng. 1(11), 195-203.

38. Panda, A., Murugan, S., Singh, R., 2016. Performance and emission characteristics of diesel fuel produced from waste plastic oil obtained by catalytic pyrolysis of waste polypropylene. Energ. Source. Part A. 38(4), 568–576.
39. Persson, H., Duman, I., Wang, S., Pettersson, L. J., Yang, W., 2019. Catalytic pyrolysis over transition metal-modified zeolites: A comparative study between catalyst activity and deactivation. J. Anal. Appl. Pyrolysis 138, 54-61.
40. PlasticsEurope, 2019. Plastics – the Facts 2019: An analysis of European plastics production, demand and waste data. https://www.plasticseurope.org/application/files/1115/7236/4388/FINAL_web_version_Plastics_the_facts2019_14102019.pdf
41. Prigiobbe, V., Polettini, A., Baciocchi, R., 2009. Gas–solid carbonation kinetics of Air Pollution Control residues for CO_2 storage. Chem. Eng. J. 148, 270–278.
42. Qureshi, M.S., Oasmaa, A., Pihkola, H., Deviatkin, I., Tenhunen, A., Mannila, J., Minkkinen, H., Pohjakallio, M., Laine-Ylijoki, J., 2020. Pyrolysis of plastic waste: Opportunities and challenges. J. Anal. Appl. Pyrol. 148, 104804.
43. Razzaq, M., Zeeshan, M., Qaisar, S., Iftikhar, H., Muneer, B., 2019. Investigating use of metal-modified HZSM-5 catalyst to upgrade liquid yield in co-pyrolysis of wheat straw and polystyrene. Fuel 257, 116119.
44. Saraçoğlu, E., Uzun, B.B., Apaydin-Varol, E., 2017. Upgrading of fast pyrolysis bio-oil over Fe modified ZSM-5 catalyst to enhance the formation of phenolic compounds. Int. J. Hydrogen Energ. 42(33), 21476–21486.

669 45. Sebestyén, Z., Barta-Rajnai, E., Bozi, J., Blazsó, M., Jakab, E., Miskolczi, N., Sója, J.,
670 Czégény, Z., 2017. Thermo-catalytic pyrolysis of biomass and plastic mixtures using HZSM-
671 5. Appl. Energ. 207, 114–122.
672 46. Seo, Y.H., Lee, K.H., Shin, D.H., 2003. Investigation of catalytic degradation of highdensity
673 polyethylene by hydrocarbon group type analysis. J. Anal. Appl. Pyrol. 70, 383–398.
674 47. Shafaghat, H., Jae, J., Jung, S.-C., Jeon, J.-K., Ko, C.H., Park, Y.-K., 2018. Effect of methane
675 co-feeding on product selectivity of catalytic pyrolysis of biomass. Catal. Today 303, 200–
676 206.
677 48. Sharuddin, S.D.A., Abnisa, F., Daud, W.M.A.W., Aroua, M.K., 2016. A review on pyrolysis
678 of plastic wastes. Energ. Convers. Manage. 115, 308–326.
679 49. Tucker, E.L., Chickering, G.W., Spreadbury, C.J., Laux, S.J., Townsend, T.G., 2020. A
680 componential approach for evaluating the sources of trace metals in municipal solid waste.
681 Chemosphere 260 (2020) 127524.
682 50. Udayanga, W.D.C., Veksha, A., Giannis, A., Liang, Y.N., Lisak, G., Hu, X., Lim, T.-T.,
683 2019. Insights into the speciation of heavy metals during pyrolysis of industrial sludge. Sci.
684 Total Environ. 691, 232–242.
685 51. Udayanga, W.D.C., Veksha, A., Giannis, A., Lisak, G., Chang, V.W.-C., Lim, T.-T., 2018.
686 Fate and distribution of heavy metals during thermal processing of sewage sludge. Fuel 226,
687 721–744.
688 52. Veksha, A., Yin, K., Moo, J.G.S., Oh, W.D., Ahamed, A., Chen, W.Q., Weerachanchai, P.,
689 Giannis, A., Lisak, G., 2020. Processing of flexible plastic packaging waste into pyrolysis oil
690 and multi-walled carbon nanotubes for electrocatalytic oxygen reduction. J. Hazard. Mater.
691 387, 121256.

53. Vichaphund, S., Aht-Ong, D., Sricharoenchaikul, V., Atong, D., 2017. Effect of CV-ZSM-5, Ni-ZSM-5 and FA-ZSM-5 catalysts for selective aromatic formation from pyrolytic vapors of rubber wastes. J. Anal. Appl. Pyrol. 124, 733–741.
54. Viet, D.B., Chan, W.-P., Phua, Z.-H., Ebrahimi, A., Abbas, A., Lisak, G., 2020. The use of fly ashes from waste-to-energy processes as mineral CO2 sequesters and supplementary cementitious materials. J. Hazard. Mater. 398, 122906.
55. Wang, J., Jiang, J., Wang, X., Pang, S., Sun, Y., Meng, X., Li, M., Ruan, R., Ragauskas, A.J., 2020. Enhanced BTEX formation via catalytic fast pyrolysis of styrene-butadiene rubber: Comparison of different catalysts. Fuel 278, 118322.
56. Wang, J., Wang, L., 2011. Catalytic Pyrolysis of Municipal Plastic Waste to Fuel with Nickel-loaded Silica-alumina Catalysts. Energ. Source. Part A. 33(21), 1940–1948.
57. Wang, S., Zhang, F., Cai, Q., Li, X., Zhu, L., Wang, Q., Luo, Z., 2014. Catalytic steam reforming of bio-oil model compounds for hydrogen production over coal ash supported Ni catalyst. Int. J. Hydrogen Energ. 39(5), 2018–2025.
58. Williams, P.T., Slaney, E., 2007. Analysis of products from the pyrolysis and liquefaction of single plastics and waste plastic mixtures. Resour. Conserv. Recycl. 51, 754–769.
59. Xin, M., Xing, E., Gao, X., Wang, Y., Ouyang, Y., Xu, G., Luo, Y., Shu, X., 2019. Ga Substitution during Modification of ZSM-5 and Its Influences on Catalytic Aromatization Performance. Ind. Eng. Chem. Res. 58, 6970-6981.
60. Yao, D., Yang, H., Chen, H., Williams, P., 2018. Investigation of nickel-impregnated zeolite catalysts for hydrogen/syngas production from the catalytic reforming of waste polyethylene. Appl. Catal. B-Environ. 227(C), 477–487.

61. Yin, K., Ahamed, A., Lisak, G., 2018. Environmental perspectives of recycling various combustion ashes in cement production – A review. Waste Manage. 78, 401–416.
62. Yin, K., Chan, W.-P., Dou, X., Ahamed, A., Lisak, G., Chang, V. W.-C., 2020a. Human exposure and risk assessment of recycling incineration bottom ash for land reclamation: A showcase coupling studies of leachability, transport modeling and bioaccumulation. J. Hazard. Mater. 385, 121600.
63. Yin, K., Dou, X., Chan, W.-P., Chang, V. W.-C., 2020b. Comparative leaching characteristics of fly/bottom ashes from municipal solid waste incineration under various environmental stresses. J. Mater. Cycles Waste. 22, 46-55.
64. Yin, K., Wang, H., Veksha, A., Dou, X., Mohamed, D.K.B., Heberlein, S., Liu, G., Chen, W., Lisak, G., 2021. Oxygen carriers from incineration bottom ash for chemical looping combustion of syngas: Effect of composition on combustion efficiency. Chem. Eng. J. 405, 127068.
65. Zhang, C., Kwak, G., Park, H.-G., Jun, K.-W., Lee, Y.-J., Kang, S.C., Kim, S., 2019. Light hydrocarbons to BTEX aromatics over hierarchical HZSM-5: Effects of alkali treatment on catalytic performance. Micropor. Mesopor. Mat. 276, 292-301.
66. Zheng, Y., Wang, F., Yang, X., Huang, Y., Liu, C., Zheng, Z., Gu, J., 2017. Study on aromatics production via the catalytic pyrolysis vapor upgrading of biomass using metal-loaded modified H-ZSM-5. J. Anal. Appl. Pyrol. 126, 169–179.
67. Zhou, J., Ma, H., Gao, M., Sun, W., Zhu, C., Chen, X., 2018. Changes of chromium speciation and organic matter during low-temperature pyrolysis of tannery sludge. Environ. Sci. Pollut. R. 25, 2495-2505.

736 68. Zhu, F., Xiong, Y., Wang, Y., Wei, X., Zhu, X., Yan, F., 2018. Heavy metal behavior in
737 "Washing-Calcination-Changing with Bottom Ash" system for recycling of four types of fly
738 ashes. Waste Manage. 75, 215-225.
739